Use of an Observation Network in the Great Basin to Evaluate Gridded Climate Data

DANIEL J. MCEVOY

Desert Research Institute, and Atmospheric Science Graduate Program, University of Nevada, Reno, Nevada

JOHN F. MEJIA AND JUSTIN L. HUNTINGTON

Desert Research Institute, Reno, Nevada

(Manuscript received 16 January 2014, in final form 24 June 2014)

ABSTRACT

Predicting sharp hydroclimatic gradients in the complex terrain of the Great Basin can prove to be challenging because of the lack of climate observations that are gradient focused. Furthermore, evaluating gridded data products (GDPs) of climate in such environments for use in local hydroclimatic assessments is also challenging and typically ignored because of the lack of observations. In this study, independent Nevada Climate-Ecohydrological Assessment Network (NevCAN) observations of temperature, relative humidity, and precipitation collected along large altitudinal gradients of the Snake and Sheep mountain ranges from water-year 2012 (October–September) are utilized to evaluate four GDPs of different spatial resolutions: Parameter–Elevation Regressions on Independent Slopes Model (PRISM) 4 km, PRISM 800 m, Daymet 1 km, and a North American Land Data Assimilation System (NLDAS)–PRISM hybrid 4-km product. Inconsistencies and biases in precipitation measurements due to station siting and gauge type proved to be problematic with respect to comparisons to GDPs. This study highlights a weakness of GDPs in complex terrain: an underestimation of inversion strength and resulting minimum temperature in foothill regions, where cold air regularly drains into neighboring valleys. Results also clearly indicate that for semiarid regions, the assumption that daily average dewpoint temperature T_{dew} equals daily minimum temperature does not hold true and should not be used to interpolate T_{dew} spatially. Comparison statistics of GDPs to observations varied depending on the climate variable and grid spatial resolution, highlighting the importance of conducting local evaluations for hydroclimatic assessments.

1. Introduction

Weather over complex terrain has been found to be particularly sensitive to small changes in climatic forcings (Loarie et al. 2009; Rangwala and Miller 2012). Therefore, weather observation networks in complex terrain are useful for studying the local effects of potential changes in regional temperature and precipitation. Globally, mountainous regions serve as the primary source of water for about 50% of the population (Bandyopadhyay et al. 1997) and nearly all of the perennial surface and groundwater resources in the Great Basin (Eakin 1966; Flint et al. 2004). The accumulation of wet season (October–March) precipitation in the form of snow comprises roughly 90% of the annual precipitation. Diffuse snowmelt during the spring provides nearly all of the annual runoff and groundwater recharge, which makes the Great Basin particularly sensitive to climatic changes (Barnett et al. 2005; Rauscher et al. 2008). With development continuing to increase in metropolitan and rural areas of the Great Basin and pending interbasin groundwater transfers planned from eastern to southern Nevada (Burns and Drici 2011; Nevada Bureau of Land Management 2012), a detailed analysis of hydroclimatic variability across altitudinal gradients in the Great Basin is needed.

Weather stations in the Great Basin are predominately located in valleys, which presents a unique challenge for studying altitudinal climatic gradients and their effects on the environment. Because climate observations are particularly sparse, gridded data products (GDPs) are used extensively by researchers and practitioners to make estimates of temperature, precipitation, and humidity distributions across space and time, despite potential large

Corresponding author address: Daniel J. McEvoy, Desert Research Institute, 2215 Raggio Pkwy., Reno, NV 89512.
E-mail: mcevoyd@dri.edu

DOI: 10.1175/JHM-D-14-0015.1

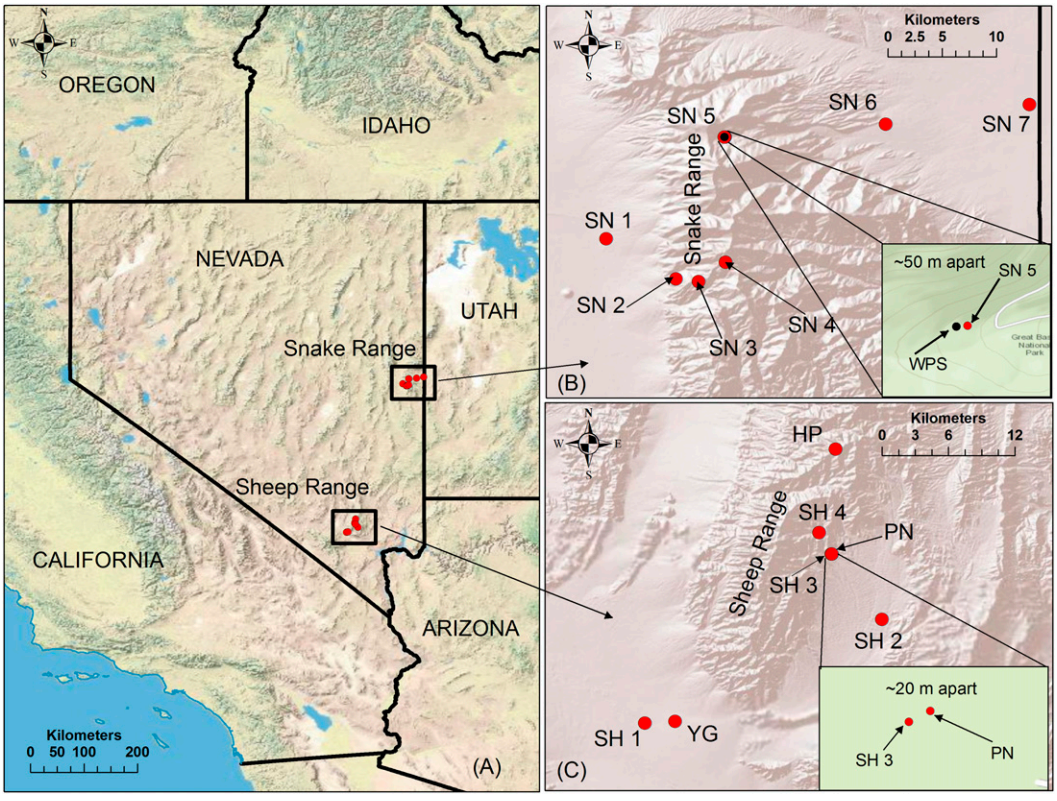

FIG. 1. (a) Study area with insets indicating locations of the Snake and Sheep Ranges. Close-up of the (b) Snake and (c) Sheep Range with red dots indicating station locations. Zoomed-in frame (b) highlights the close proximity of WPS to NevCAN. Station summaries can be found in Table 1.

uncertainties. In the Great Basin and surrounding regions, Parameter–Elevation Regressions on Independent Slopes Model (PRISM; Daly et al. 1994) products are commonly used for research and applied studies related to ecology (Ackerly et al. 2010), biology (Bradley 2009; Leger 2013), hydrology (Welch et al. 2007; Burns and Drici 2011; Huntington and McEvoy 2011; Huntington and Niswonger 2012; McEvoy et al. 2012; Feld et al. 2013), climatology (Porinchu et al. 2010), and meteorology (Lundquist et al. 2010). Of particular importance is the fact that over the last 10 years, PRISM precipitation products have also been used in most expert witness studies and reports associated with major water rights hearings in Nevada, where uncertainty of PRISM is commonly a central focus for assessing uncertainty in the perennial yield of groundwater (Jeton et al. 2006; Lundmark et al. 2007; Zhu and Young 2009; Epstein et al. 2010; Burns and Drici 2011; Nevada State Engineer's Office 2012). Gridded data products are often used without comparing estimates to independent or dependent observations (Bradley 2009; Ackerly et al. 2010; Porinchu et al. 2010; Leger 2013). Therefore, studies that utilize independent observations collected along mountain transects can prove to be valuable for validation of GDPs, as well as revealing physical phenomena related to altitudinal gradients, such as location of maximum precipitation, orographic processes, temperature and vapor lapse rates, and spatial variability related to wind and topographic characteristics such as slope and aspect.

The Nevada Climate-Ecohydrological Assessment Network (NevCAN), located in eastern and southern Nevada (Fig. 1), is a new observation network designed to assess climate variability and change and associated impacts on the surrounding ecology and hydrology (Mensing et al. 2013). The network consists of one west–east transect in eastern Nevada (Snake Range) and one south–north transect in southern Nevada (Sheep Range; Fig. 1). With records beginning in June 2010, observations from NevCAN have not been assimilated into the generation of GDPs, so a novel GDP validation can be conducted with independent observations. In describing guidelines for assessing modeled spatial climate datasets, Daly (2006) notes that using data independent of the model will provide the least biased evaluation. In this study, we use acquired NevCAN data as the independent dataset to evaluate four GDPs with different spatial resolutions. Using different spatial resolutions of 4 km, 1 km, and 800 m provides beneficial insight into

disparities among the different GDPs, observations, and the ability of GDPs to resolve local-scale precipitation, temperature, and humidity features.

An important, yet often overlooked, aspect of comparing any estimated weather data to observations is the acknowledgment of measurement uncertainties. Measuring solid precipitation remains particularly challenging and automated systems have been found to undermeasure by as much as 20%–50%, mostly due to gauge undercatch from strong winds (Rasmussen et al. 2012). Weather station siting and gauge type can also impact measured precipitation totals (PPT), especially during snowfall events (Goodison et al. 1998; Yang et al. 1998; Fassnacht 2004). Therefore, biases in observed precipitation should be established and taken into consideration before analyzing differences between GDPs and measurements.

As highlighted above, an abundance of dynamically and statistically derived gridded precipitation and temperature products are available to help overcome observational limitations (Daly et al. 1994; Thornton et al. 1997; Abatzoglou 2013). Our first objective is to understand and acknowledge the degree to which these products can satisfactorily resolve altitudinal climatic gradients in complex terrain and at what resolution. The second objective of this study is to assess the uncertainties associated with precipitation measurements and the impacts on the comparisons to estimated GDPs.

In the following sections, we describe the NevCAN transects, additional observations, and GDPs, as well as the analyses and statistics used for the comparisons and quality-assured and quality-controlled protocols used to assess observational uncertainty and error (section 2). The results of the measurement uncertainty analysis and comparisons between GDPs and observations are presented (section 3) and discussed with respect to altitudinal gradients and systematic biases found in estimated and measured temperature, precipitation, and humidity. Finally, we summarize and discuss our results and provide concluding remarks on the differences between GDPs and observations and how the differences vary with grid size, parameter, and altitude (section 4).

2. Data and methodology

a. NevCAN data

The NevCAN meteorological data were obtained from the Western Regional Climate Center (WRCC; www.wrcc.dri.edu/SRtransect/; www.wrcc.dri.edu/GBtransect/) for the water-year 2012 (from 1 October 2011 through 30 September 2012), and site descriptions are shown in Table 1. Alternatively, NevCAN data can be obtained from the Nevada Climate Change Portal (http://sensor.nevada.

TABLE 1. Summary of station locations, elevations, measured variables (where *T* indicates temperature), sampling frequency, and precipitation gauge information.

Range	Site	Network	Lat (°N)	Lon (°W)	Elev (m)	Variables	Sampling frequency	Precipitation gauge type	Orifice size (mm)	Alter shield
Snake	Sagebrush west (SN 1)	NevCAN	38.9256	114.4078	1768	PPT, *T*, RH	10 min	TB and weighing	TB (150) weighing (160)	TB (no) weighing (yes)
	Pinyon Juniper west (SN 2)	NevCAN	38.8922	114.35	2202	PPT, *T*, RH	10 min	TB and weighing	TB (150) weighing (160)	TB (no) weighing (yes)
	Montane west (SN 3)	NevCAN	38.89	114.3314	2819	PPT, *T*, RH	10 min	TB and weighing	TB (150) weighing (160)	TB (no) weighing (yes)
	Subalpine west (SN 4)	NevCAN	38.9061	114.3089	3554	PPT, *T*, RH	10 min	TB and weighing	TB (150) weighing (160)	TB (no) weighing (yes)
	Subalpine east (SN 5)	NevCAN	39.01	114.3094	3081	PPT, *T*, RH	10 min	TB and weighing	TB (150) weighing (160)	TB (no) weighing (yes)
	Sagebrush east (SN 6)	NevCAN	39.0206	114.1764	1840	PPT, *T*, RH	10 min	TB and weighing	TB (150) weighing (160)	TB (no) weighing (yes)
	Salt Desert Shrub east (SN 7)	NevCAN	39.0369	114.0572	1580	PPT, *T*, RH	10 min	TB and weighing	TB (150) weighing (160)	TB (no) weighing (yes)
	Wheeler Peak (WPS)	SNOTEL	39.00995	114.31	3085	PPT, *T*	Hourly	Weighing	305	Yes
Sheep	Desert Shrub (SH 1)	NevCAN	36.4353	115.3558	893	PPT, *T*, RH	10 min	TB	200	Yes
	Blackbrush (SH 2)	NevCAN	36.5197	115.1633	1680	PPT, *T*, RH	10 min	TB	200	Yes
	Pinyon Juniper (SH 3)	NevCAN	36.5728	115.2042	2065	PPT, *T*, RH	10 min	TB	200	Yes
	Montane (SH 4)	NevCAN	36.5903	115.2142	2272	PPT, *T*, RH	10 min	TB and weighing	TB (200) weighing (160)	TB (no) weighing (yes)
	Yucca Gap (YG)	RAWS	36.4367	115.3314	969	PPT, *T*, RH	Hourly	TB	200	No
	Hayford Peak (HP)	SCAN	36.6581	115.201	3013	PPT, *T*, RH	Hourly	TB	200	No

TABLE 2. Geonor rain gauge and TB rain gauge comparison statistics. Diff given as Geonor minus TB and proportion of total shown with respect to Geonor seasonal total.

Season	Statistic	SN1	SN2	SN3	SN4	SN5[a]	SN6[b]	SN7[a]	SH4[c]
Cold (Oct–Mar)	R^2	0.67	0.25	0.03	No TB data	0.01	0.24	0.87	0.12
	Diff (mm)	13.91	49.3	118.13	No TB data	186.32	8.36	12.92	12.63
	Proportion of total (%)	16	32	51	No TB data	64	11	17	12
Warm (Apr–Sep)	R^2	0.98	0.97	0.78	No TB data	No TB data	No TB data	No TB data	0.91
	Diff (mm)	23.26	19.73	9.98	No TB data	No TB data	No TB data	No TB data	2.78
	Proportion of total (%)	21	12	5	No TB data	No TB data	No TB data	No TB data	1

[a] Complete data from 1 Oct to 28 Feb of cold season only.
[b] Complete data from 1 Oct to 17 Feb of cold season only.
[c] Complete data for all of cold season and from 1 Apr to 15 Aug of warm season.

edu/NCCP/Climate%20Monitoring/Network.aspx). The orientation and design of the Snake Range transect is west-to-east and south-to-north for the Sheep Range (Fig. 1). For each of the two transects, daily maximum temperature T_{max} and daily minimum temperature T_{min} and 10-min-averaged relative humidity RH and temperature were obtained. Measurement of near-surface vapor pressure e_a and dewpoint temperature T_{dew} are often neglected in mountain observing networks [i.e., Snowpack Telemetry (SNOTEL)] but are crucial for estimating evapotranspiration, atmospheric water demand, and land surface and boundary layer feedbacks, which are often required for hydrologic and ecological modeling (Crago et al. 2010; Huntington et al. 2011; Feld et al. 2013). Here, we compute e_a and T_{dew} from 10-min RH and temperature data, which are then averaged to daily and monthly time steps to compare against GDPs. Dewpoint was calculated from actual vapor pressure following the Murray (1967) equation. Actual vapor pressure was derived from saturation vapor pressure e_s (a function of air temperature) and RH as follows: $e_a = e_s(\mathrm{RH}/100)$. All observations were quality assured and controlled by manual inspection and then aggregated to monthly time steps for monthly comparisons of GDP.

Precipitation can be highly variable over short temporal scales; therefore, raw 10-min data were summed to the day instead of using the WRCC precomputed daily precipitation as an additional quality-assurance and quality-control measure. At the Snake Range, each station is equipped with two precipitation gauge systems: 1) a weighing gauge with a 160-mm orifice diameter (Geonor T-200B) and 2) a tipping bucket (TB) with a 150-mm orifice diameter [Texas Electronics (TE) 525]. At the Sheep Range, all stations are equipped with tipping buckets (TB4; 200-mm orifice diameter) except for the Montane station (SH4), which is the only station to have both types of gauges. At locations with both types of gauges, only the Geonor gauges are equipped with Alter shields (Alter 1937) to reduce gauge undercatch, while the tipping buckets were left unshielded. Alter shields were installed at tipping bucket–only sites in the Sheep Range.

Tipping buckets are known to underestimate precipitation, especially during heavy rainfall or light drizzle (e.g., Humphrey et al. 1997), and have been shown to collect much less frozen precipitation than standard weighing gauges (e.g., Rasmussen et al. 2012). Daily tipping-bucket precipitation measurements were compared to coincident Geonor measurements of precipitation and the coefficient of determination R^2 and season total differences were computed at each station for cold and warm seasons (Table 2). During the cold season, tipping buckets consistently underestimated precipitation totals with differences exceeding 100 mm at SN3 and SN5, and R^2 was found to decrease (R^2 range of 0.01–0.87), with an exceptionally weak relationship found between the two gauge types at high elevation (R^2 of 0.01 at SN5). As expected, correlations of daily precipitation were much higher during the warm season (R^2 range of 0.78–0.98), but decreased with elevation because of more days with frozen precipitation. The lower correlations of daily precipitation during the cold season are primarily caused by a delay in timing of tip counts because of frozen precipitation events. For example, snow or ice in the tipping buckets may take from several hours to several days to melt, and the event is then offset from the Geonor data by one or several days (Fig. 2). Because of the well-known limitations of tipping buckets (e.g., Humphrey et al. 1997; Rasmussen et al. 2012), and as highlighted in this analysis, weighing gauge precipitation measurements were used for evaluating the skill of GDP precipitation estimates when available.

b. Additional observations

We utilize a Natural Resources Conservation Service (NRCS) SNOTEL station (T_{max}, T_{min}, and precipitation) to compare to a nearby (~50 m) NevCAN Snake Range station located in the high-elevation subalpine region along with all GDPs. The Wheeler Peak SNOTEL (WPS) precipitation gauge is a weighing-type gauge; however, the orifice diameter is approximately twice the size (~305 mm) of the NevCAN Geonor

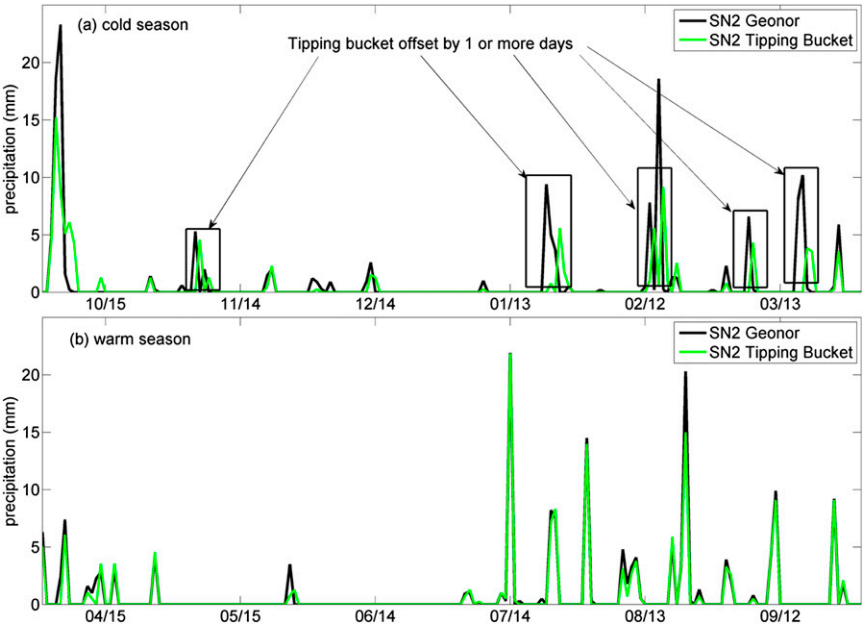

FIG. 2. Time series of Geonor rain gauge (black line) and tipping-bucket rain gauge (green line) precipitation at SN2 during the (a) cold and (b) warm season. Abscissa tick marks indicate date (month and day).

(~160 mm). Daily T_{max}, T_{min}, and precipitation SNOTEL data were obtained from the NRCS (www.wcc.nrcs.usda.gov/nwcc/site?sitenum=1147&state=nv) and aggregated to monthly time steps and quality assured and controlled.

It was determined that the WPS station is the only high-elevation station in the Snake Range being used as a control point for PRISM and Daymet spatial distribution algorithms (M. Halbleib 2013, Oregon State University, electronic communication, http://daymet.ornl.gov/overview). Therefore, the effect of dependent versus independent observations compared to GDPs is examined. In this portion of the study, we highlight the importance of thoroughly understanding the GDP control point when using GDP estimates for local climate assessments. Important assumptions related to weather station and precipitation gauge footprint, siting and exposure, and sensor limitations/deficiencies are also explored.

Two additional stations were used in the Sheep Range in order to develop a more complete south–north transect with one station from the NRCS Soil Climate Analysis Network (SCAN) (Fig. 1, Table 1). Hourly RH, temperature, and precipitation data were downloaded (www.wcc.nrcs.usda.gov/scan/) and quality assured and controlled. The Hayford Peak (HP) SCAN station is equipped with an unheated tipping bucket and has an 8-in. (~200 mm) orifice diameter. Therefore, the winter precipitation data contain large uncertainties because of tipping-bucket deficiencies described in section 2a. The Yucca Gap (YG) Remote Automatic Weather Station (RAWS) was the second additional station used at the Sheep Range, and hourly RH, temperature, and precipitation data were downloaded from WRCC (www.raws.dri.edu/cgi-bin/rawMAIN.pl?nvNYUC) and quality assured and controlled. Yucca Gap is also instrumented with an unheated tipping-bucket precipitation gauge; therefore, winter precipitation values are highly uncertain and are discussed later. Dewpoint and vapor pressure were computed following the same methods used for NevCAN data. All observations used in the study are summarized in Table 1.

c. *Gridded data*

In this study, NevCAN datasets are considered to be "baseline measurements" to evaluate the skill of four GDPs: 1) PRISM 4 km (Daly et al. 1994), 2) PRISM 800 m (Daly et al. 1994), 3) Daily Surface Weather and Climatological Summaries (hereafter called Daymet) 1 km (Thornton et al. 1997), and 4) a North American Land Data Assimilation System (NLDAS)–PRISM hybrid 4 km (hereafter called JA; Abatzoglou 2013). We address the uncertainties in NevCAN precipitation measurements and highlight how these biased observations impact the comparisons to GDPs in section 3.

Total monthly PRISM precipitation and average monthly T_{max}, T_{min}, and T_{dew} were obtained (acquired in January 2013) for both 800-m and 4-km spatial resolutions

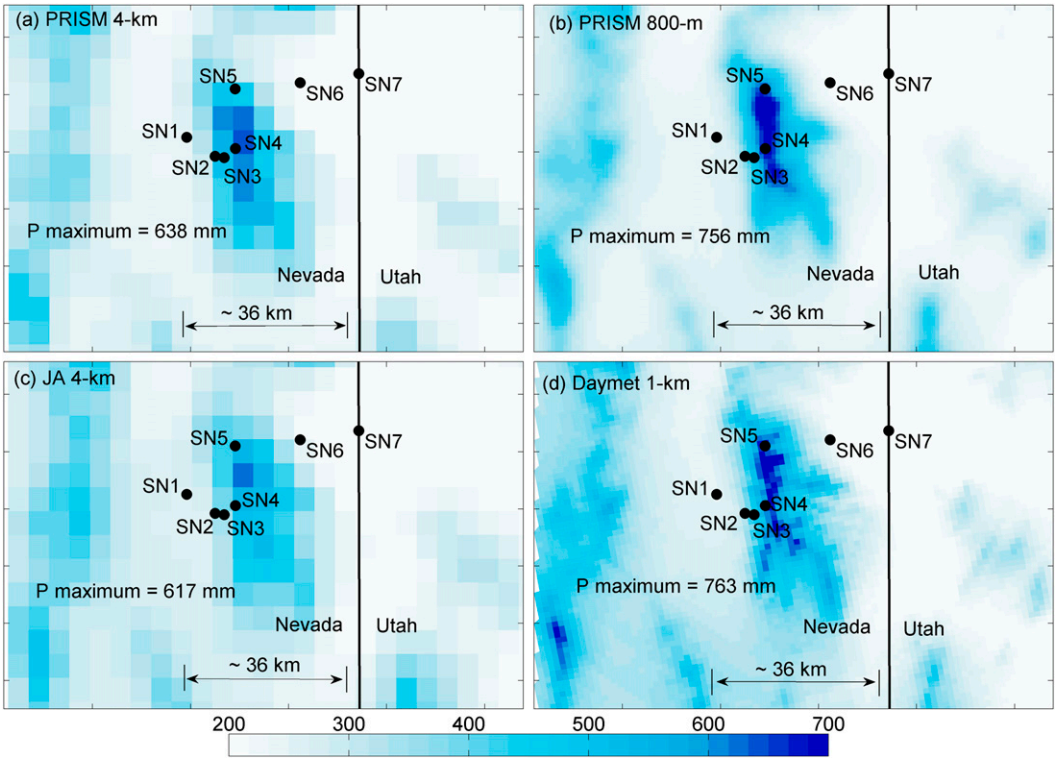

FIG. 3. Water-year 2012 total precipitation (mm) at the Snake Range for (a) PRISM 4 km, (b) PRISM 800 m, (c) JA 4 km, and (d) Daymet 1 km.

from the PRISM website (www.prism.oregonstate.edu). All PRISM variables were interpolated using climatologically aided interpolation (CAI; Willmott and Robeson 1995). For T_{max}, T_{min}, and precipitation, PRISM was used to interpolate 1971–2000 monthly normals, using elevation as the predictor grid, with stations weighted by vertical and horizontal distance, plus several physiographic factors, such as topographic orientation, coastal proximity, inversion height, and topographic position (Daly et al. 2008). Once the normals were interpolated, CAI was used to interpolate data for a given month and year. Average monthly PRISM T_{dew} estimates were computed by first taking monthly dewpoint depression K_o observations and spatially interpolating monthly K_o using PRISM T_{min} as the predictor in the regression function. Dewpoint was then back calculated using PRISM K_o and T_{min} (C. Daly 2012, Oregon State University, personal communication). To create the monthly dewpoint time series, CAI was again used; PRISM assimilated station data in the form of monthly mean dewpoint and used the 1971–2000 normal dewpoint for that month as the predictor grid in its local regression function. The Murray (1967) equation was rearranged and used to compute vapor pressure, where $e_a = \exp[(0.0707T_{dew} - 0.492\,99)/(0.004\,21T_{dew} + 1)]$.

The third GDP evaluated was developed by Abatzoglou (2013) and combines the spatial attributes of monthly PRISM data with daily temporal resolution from phase 2 of NLDAS (NLDAS-2; Mitchell et al. 2004). All of the NLDAS-2 nonprecipitation surface variables are derived from the North American Regional Reanalysis (NARR; Mesinger et al. 2006), and the native NARR data are spatially downscaled from 32 to 12 km and temporally disaggregated from 3-hourly to hourly (Cosgrove et al. 2003). For NLDAS-2 precipitation, Climate Prediction Center (CPC) gridded daily gauge data (with a PRISM topographical adjustment) are the primary data source. Daily CPC data are temporally disaggregated to hourly using radar and satellite-based estimates (if available) and NARR. The first step in developing JA data is a bilinear interpolation of NLDAS-2 onto the PRISM grid (4 km). Climatologically aided interpolation is then used to bias correct the daily temperature, humidity, and precipitation data to a given PRISM month (Abatzoglou 2013). Daily T_{max}, T_{min}, maximum RH (i.e., RH_{max}), minimum RH (i.e., RH_{min}), and total precipitation were obtained from an online dataset (http://cloud.insideidaho.org/data/epscor/gridmet/). Dewpoint from JA was calculated at the daily time step as a function of actual vapor pressure following the Murray (1967) equation. Actual vapor pressure was derived from RH_{max}, RH_{min},

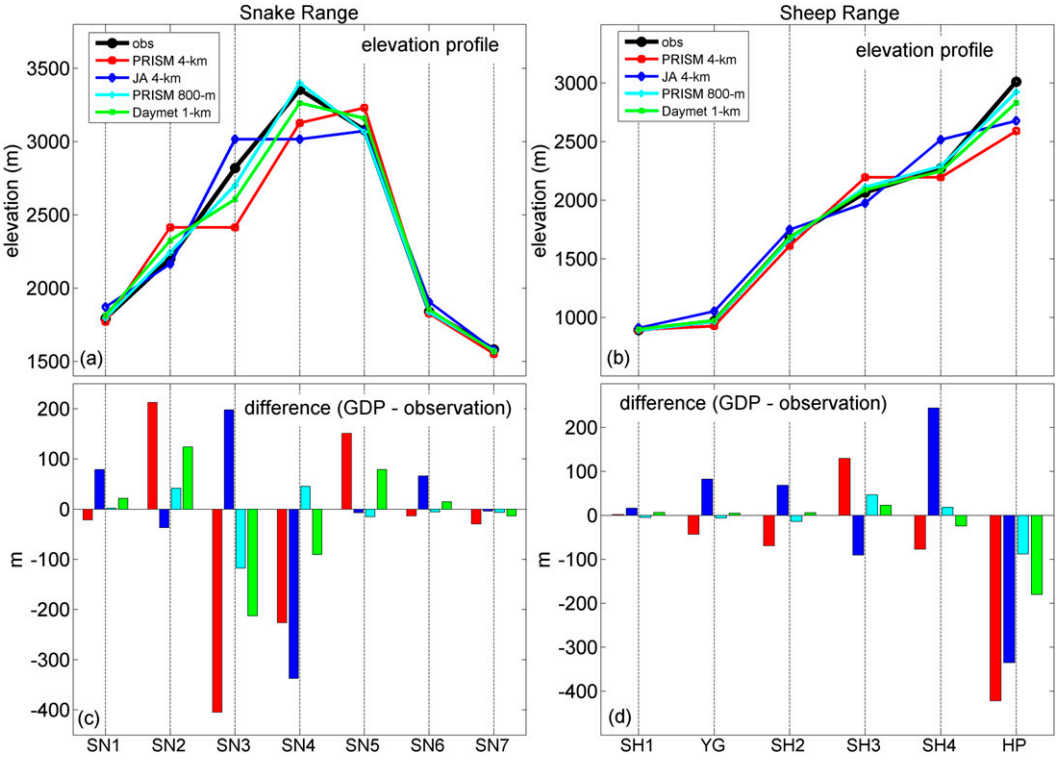

FIG. 4. Elevation of each station and nearest GDP pixel for (a) Snake and (b) Sheep Ranges. (c),(d) Differences between grid point and station elevation (GDP station). The *x* axis follows the dominant alignment, in the west–east direction for the Snake Range and nearly south–north for the Sheep Range.

saturation vapor pressure at $T_{\max}$ $e_{s_{T_{\max}}}$, and saturation vapor pressure at $T_{\min}$ $e_{s_{T_{\min}}}$, where $e_a = \{[e_{s_{T_{\max}}}(\mathrm{RH_{min}}/100)] + [e_{s_{T_{\min}}}(\mathrm{RH_{max}}/100)]\}/2$, as recommended by Allen et al. (1998) for daily data.

Daymet was the fourth GDP evaluated and is available for all of North America at daily time steps and at 1-km spatial resolution. Daily $T_{\max}$, $T_{\min}$, precipitation, and vapor pressure data were acquired online (http://daymet.ornl.gov; Thornton et al. 2014). To interpolate $T_{\max}$, $T_{\min}$, and precipitation, Daymet uses a truncated Gaussian filter, and a weighted least squares regression is applied to establish the relationship between a given variable and elevation (Thornton et al. 1997). While both Daymet and PRISM use local linear regression, Daymet assumes a strictly monotonic relationship between temperature and elevation, which limits the ability of Daymet to handle temperature inversions (Daly 2006). Daymet daily average vapor pressure is derived following the assumption that daily $T_{\min}$ equals daily average T_{dew} (Thornton and Running 1999; Thornton et al. 2000). However, as we show in section 3, Daymet monthly average T_{dew} rarely equals $T_{\min}$, especially in semiarid and arid environments. Daily average T_{dew} was calculated directly from Daymet daily average vapor pressure following Murray (1967).

Figure 3 provides a spatial perspective on grid resolution of different GDPs in relation to station density and illustrates the water-year 2012 total precipitation at the Snake Range. Although all GDPs indicate maximum precipitation occurring near the crest of the Snake Range (SN4 and SN5), PRISM 4 km and JA both have a maximum value of over 100 mm less than PRISM 800 m and Daymet. A coarser grid size leads to larger areas per pixel being averaged. Therefore, mountain peaks are represented as lower-elevation areas when compared to 800-m and 1-km DEM values and precipitation totals are reduced. A more detailed discussion on the effects of grid resolution on biases is presented in section 3.

d. GDP–observation comparison and statistical methods

For each observing station, the nearest GDP center point was found to conduct direct comparisons for each meteorological variable, as well as elevation (Fig. 4). Given that GDPs largely rely on elevation to distribute climatic variables, differences between GDP pixel and station elevations were expected to largely explain GDP biases. For example, Fig. 4 shows the PRISM 4-km pixel at SN2 to be more than 200 m higher than the station

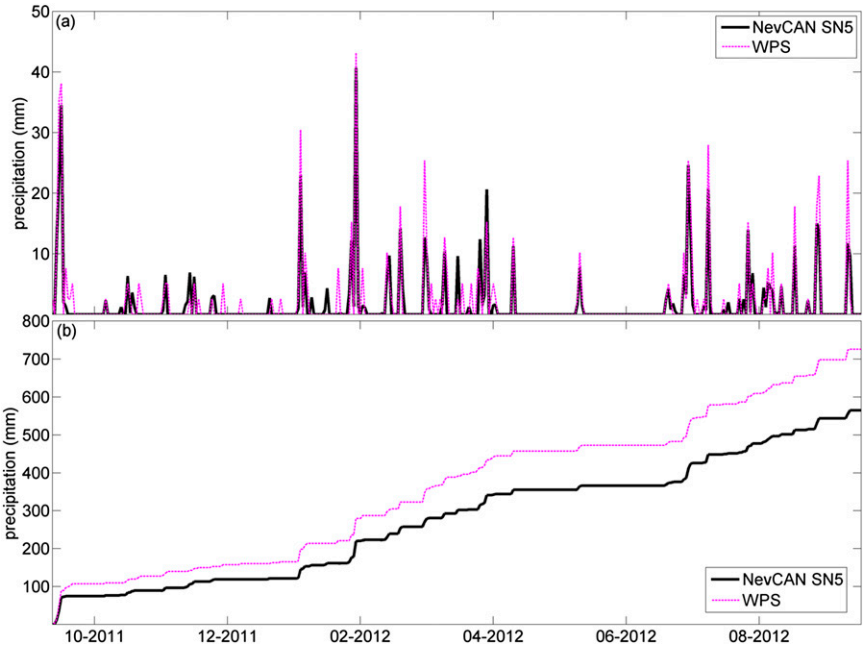

FIG. 5. NevCAN SN5 (black) and WPS (magenta) (a) daily PPT and (b) accumulated precipitation throughout the water year. Abscissa tick marks indicate date (month and year).

elevation. Based on this alone, PRISM 4-km temperature was expected to be cooler and precipitation was expected to be greater than SN2 observed values because of environmental lapse rates and typical midlatitude precipitation–elevation relationships, where precipitation increases with elevation (Houghton 1979; Smith 1979; Daly et al. 1994). Biases between station observations and GDPs were computed using seasonal means for T_{max}, T_{min}, and T_{dew} and sums for precipitation. Additionally, R^2 and mean absolute error (MAE) were computed using daily means and sums (for JA and Daymet GDPs). All biases were computed as GDP minus observation.

3. Results

a. Snake Range SN5 and WPS intercomparison

An important aspect of any comparison study between estimated and measured data is an evaluation, or at least an acknowledgment, of the quality of the measured data. For this study, we compare measured precipitation at the NevCAN SN5 station to measured precipitation at the WPS station. The distance between the two stations is ~50 m with an elevation difference of only 3.7 m. Daily and water-year accumulation of precipitation for SN5 and WPS are shown in Fig. 5, which clearly shows that both stations tend to record the same precipitation events; however, WPS consistently has higher daily totals. It seems unrealistic that WPS would receive ~30% more precipitation in one water year than SN5, considering their close proximity (~50 m apart) and nearly identical elevation.

There are a number of factors that could contribute to these contrasting values that fall within two general categories: 1) instrumentation differences and 2) station siting. Both gauges are weighing types and have Alter shields, and the orifice heights for WPS and SN5 are 4.9 and 3 m, respectively, with the WPS orifice diameter being twice that of SN5 (diameters of 305 and 160 mm, respectively). The higher orifice height at WPS should experience higher wind speed, and therefore less catch, when compared to SN5, which is in contrast to our findings. However, siting characteristics, such as the height of surrounding vegetation and exposure to wind, could also be affecting precipitation totals, particularly during snowfall events (Goodison et al. 1998; Yang et al. 1998; Fassnacht 2004). Photographs from SN5 reveal large, tightly spaced trees surrounding the shielded Geonor gauge (Figs. 6a,b), and the gauge height is low with respect to surrounding tree height, while the tree spacing around the WPS gauge appears to be much less dense (Figs. 6c,d). The prevailing wind direction in the winter months is from the west-southwest, and the clusters of large trees surrounding SN5 (specifically the clusters to the west of the gauge; Fig. 6b) are likely physically blocking wind-blown snow from being captured in the gauge, whereas less dense forest lies directly to the west

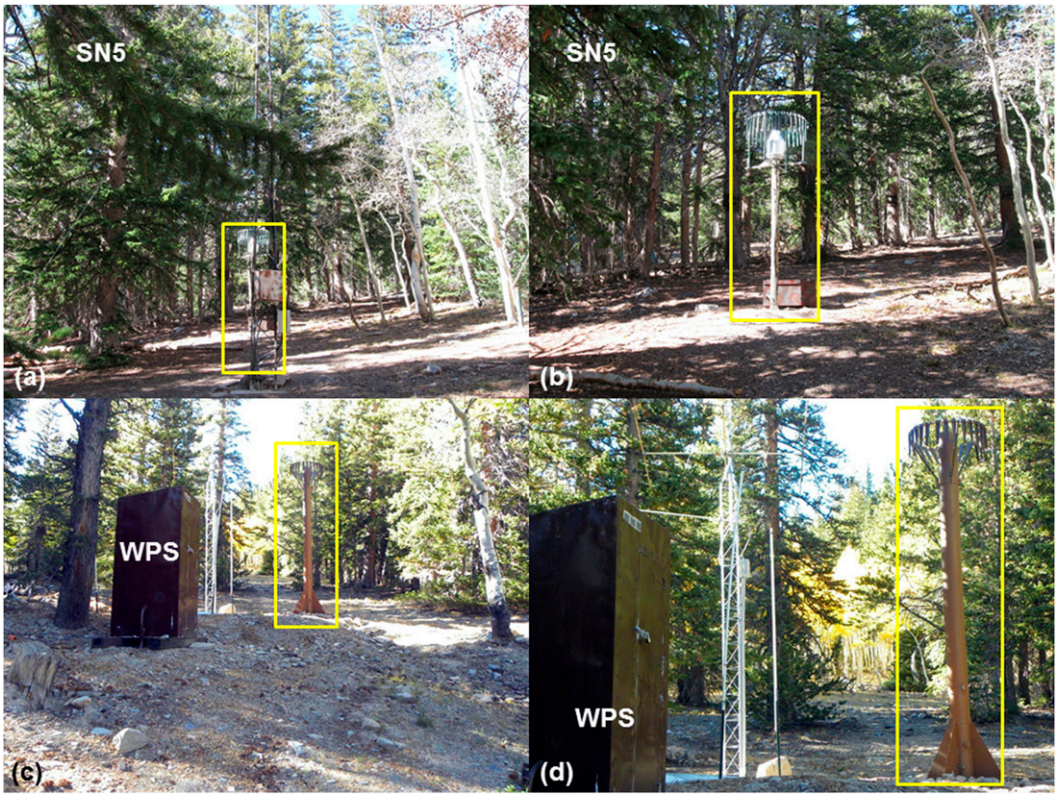

FIG. 6. Photographs of the SN5 Geonor gauge and the surrounding vegetation, looking to the (a) east and (b) west. (c),(d) Photographs of the WPS weighing gauge and surrounding vegetation. Rain gauges are highlighted by yellow rectangles. The orientation of (c) and (d) is unknown. Photographs courtesy of WRCC and NRCS.

of WPS (not shown; can be seen from satellite imagery using Google Earth). It should also be noted that the SNOTEL gauge reports precipitation to the nearest tenth of an inch, while the Geonor reports to the nearest hundredth of an inch, indicating less uncertainty in the precipitation that is caught by the NevCAN gauges. Differences in gauge calibration could also lead to different precipitation measurements for similar events (Sieck et al. 2007), which may be yet another factor leading to the discrepancies identified in this section.

Inconsistencies and biases in measurements due to station siting, calibration, and design are problematic if used for impact assessments and reports. Through the intercomparison of SN5 and WPS, we have shown that great uncertainty remains with respect to precipitation measurements in this region, and the resulting comparisons to GDPs will also contain a large degree of uncertainty. Unfortunately, a comparison such as we have presented here is not possible with other NevCAN stations.

b. *Snake Range comparisons of observations and GDPs*

Cold season (October–March) and warm season (April–September) precipitation totals and mean T_{max}, T_{min}, and T_{dew} values for station observations and GDPs over the Snake Range are shown in Fig. 7. Typical valley–mountain precipitation gradients were observed with NevCAN measurements and GDP estimates, with seasonal totals increasing from west to east, and then decreasing from the crest to the eastern valley floor (Figs. 7a,b). The NevCAN maximum measured precipitation during the cold season occurs at SN4 (297 mm), which is located on the windward side of the Snake Range at a slightly higher elevation than SN5, which is located on the lee side. The SN4 site is situated near a ridge line and the surrounding vegetation is smaller and much less dense when compared to the vegetation surrounding SN5. The WPS station recorded a much greater amount of cold season precipitation (389 mm) compared to SN5 (292 mm), which would result in the greatest cold season precipitation occurring on the lee slope. Based on these observations (NevCAN and SNOTEL), great uncertainty remains as to where the true precipitation maximum is occurring in the Snake Range. Similar observed precipitation characteristics were found during the warm season.

Gridded data seasonal precipitation totals were generally found to be higher than NevCAN observed totals

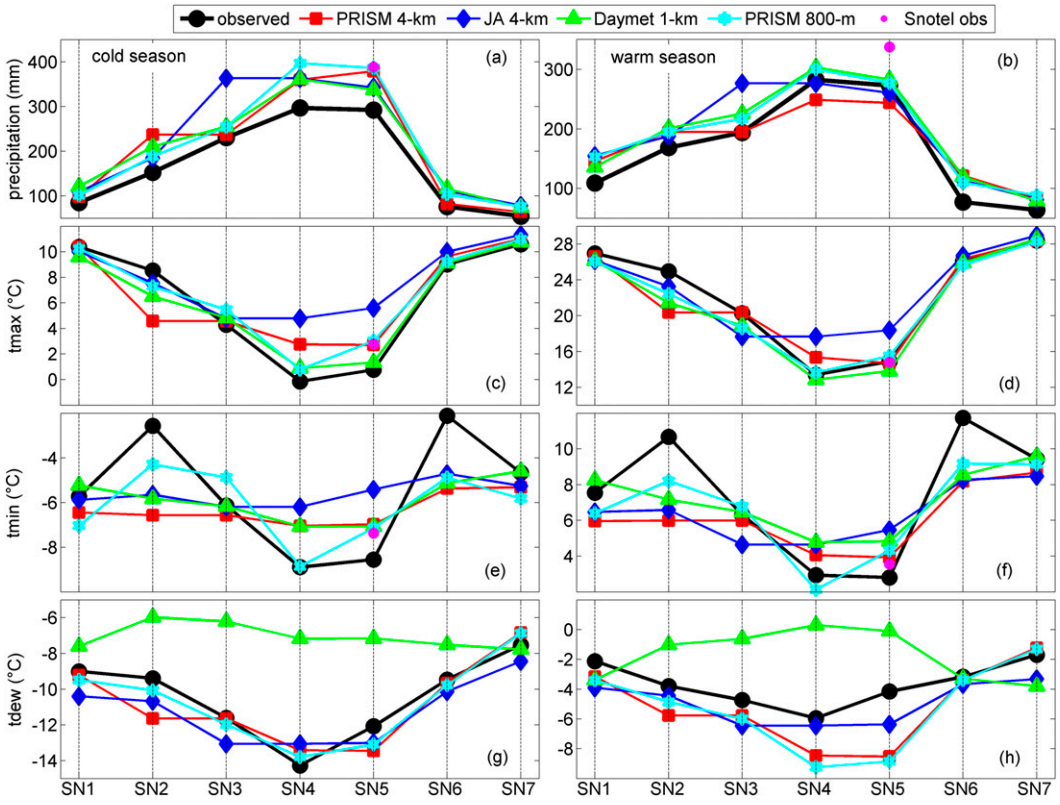

FIG. 7. Snake Range seasonal (a),(b) PPT and mean (c),(d) T_{max}; (e),(f) T_{min}; and (g),(h) T_{dew} for (left) cold and (right) warm season. The x axis is aligned west–east (from left to right).

(Figs. 8a,b). During the cold season, differences ranged from 132.8 (JA at SN3) to 6.0 mm (PRISM 800 m at SN6), and negative differences were never observed. When compared to WPS (as opposed to SN5), all GDP differences (GDP minus observations) were negative and the smallest differences were found with PRISM 800 m and 4 km (−2.3 and −9.4 mm, respectively). The positive differences found between GDPs and NevCAN stations appear to be a result of WPS being the only high-elevation control point in the area for GDPs in the Snake Range. Differences between station and gridpoint elevation could not explain the corresponding precipitation differences. For example, at SN3, the PRISM 4-km grid cell was approximately 400 m lower than the station, but precipitation was always greater than observed. Overall for precipitation comparisons, GDP performance was inconsistent, and it was found that finer grid resolution did not always lead to smaller differences between GDPs and observations.

Maximum temperature biases (Figs. 8c,d) ranged from 4.9° (JA) to −4.6°C (PRISM 4 km) for cold and warm seasons. Large negative biases (colder than observed) were found at the low-elevation sites of SN1 and SN2. These biases are directly related to differences between GDP and station elevations, with SN1 and SN2 gridpoint elevations being higher than station elevations. However, several occurrences were found where GDP elevations were higher than station elevations and positive biases (warmer) were found, as well as where lower gridpoint elevations relative to the station elevations had negative biases. For example, the PRISM 4-km grid point at SN5 is 151 m higher than the SN5 station elevation, and a positive bias of 3.6°C was found during the cold season.

NevCAN minimum temperature altitudinal gradients (Figs. 7e,f) varied from those of T_{max} in that the two alluvial fan "foothill" stations (SN2 and SN6) were warmer on average when compared to the neighboring valley floor stations (SN1 and SN7) during both seasons. Previous studies have found that, in complex terrain, T_{min} can vary greatly depending on station siting and associated local atmospheric decoupling and cold air drainage (Daly et al. 2010; Holden et al. 2011). During the nighttime hours, as the boundary layer stabilizes (typically during clear sky conditions), cold air sinks and tends to pool in low-lying areas, leading to temperature inversions near the surface and warmer conditions in foothill locations (Gustavsson et al. 1998). The ability of

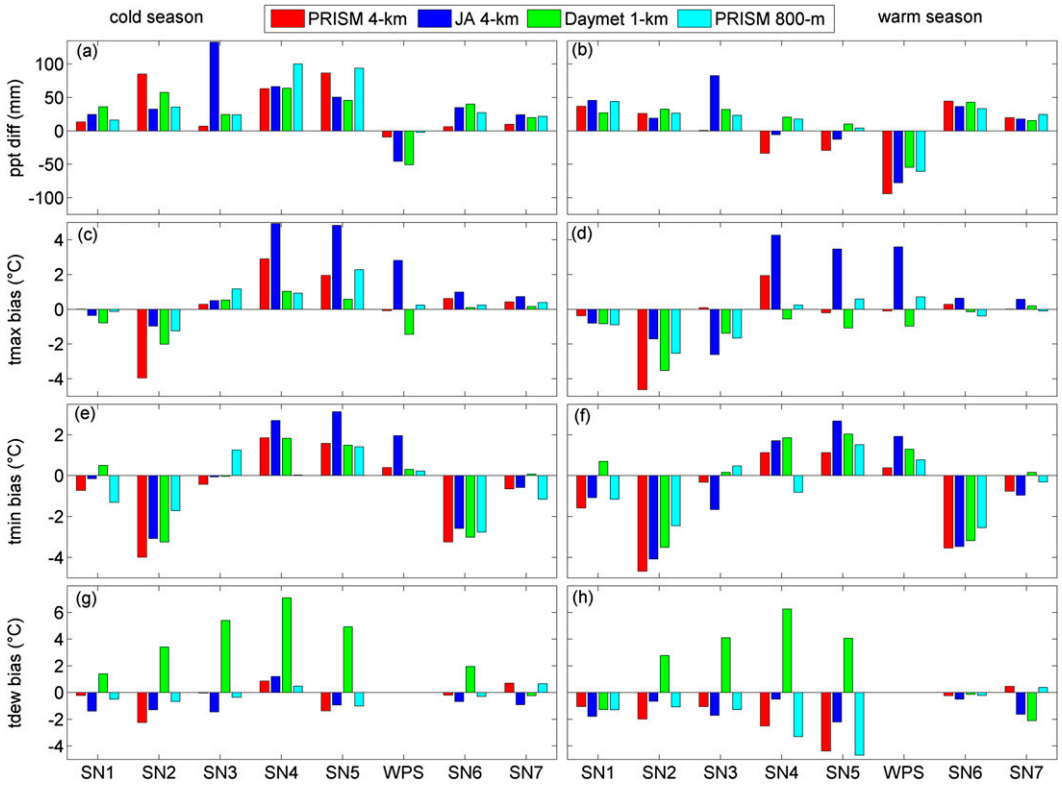

FIG. 8. Snake Range seasonal bias (GDP minus obs) for (left) cold and (right) warm season (a),(b) PPT; (c),(d) T_{max}; (e),(f) T_{min}; and (g),(h) T_{dew}. Variables needed to calculate T_{dew} are not measured at WPS; therefore, no T_{dew} values are shown.

GDPs to capture this feature was variable, with PRISM 800-m being the only GDP to capture the inversions at SN2 and SN6 during both seasons, which is a result of PRISM's use of inversion height, topographic position, and varying slopes with elevation (Daly et al. 2008). In some instances, PRISM 4 km and JA were able to represent inversions, but the magnitudes were much smaller than observed. These results highlight the need for improved methods of interpolating T_{min} observations over complex terrain.

Biases in T_{min} (Figs. 8e,f) ranged from 3.1° (JA) to −4.7°C (PRISM 4 km), with biases being generally slightly larger during the warm season. Although some of the biases can be attributed to grid point and respective station elevation differences, the large T_{min} biases at SN2 and SN6 are a result of GDPs not being able to replicate the inversion strength between valley floor and alluvial fan locations. Local lapse rates of monthly T_{min} (not shown) between SN1 and SN2 and between SN7 and SN6 averaged over the water year were +7.6° and +9.4°C km^{-1}, respectively, and were largely underestimated by GDPs (PRISM 800 m was the closest to observations with water-year average T_{min} lapse rates of +5.1° from SN1 to SN2 and +1.9°C km^{-1} from SN7 to SN6).

With a general lack of humidity observations, relatively little is known about the spatial behavior of near-surface humidity over complex terrain and the skill of GDPs to estimate humidity. As expected, we found NevCAN station seasonal average T_{dew} to decrease with altitude (Figs. 7g,h). Except for Daymet, differences between GDP and observed T_{dew} were generally small during the cold season (Figs. 7g, 8g) and ranged from −2.3° to 1.2°C, whereas warm season biases (Figs. 7h, 8h) were larger and primarily negative, ranging from −4.7° to 0.5°C. All GDPs, except for Daymet, showed the same trends with altitude. Daymet estimated nearly constant T_{dew} with respect to altitude during the cold season (Fig. 7g) and increasing T_{dew} with elevation during the warm season (Fig. 7h). The lack of skill shown by Daymet is primarily due to the underlying assumption that daily average T_{dew} is equal to T_{min}. This assumption is sometimes reasonable in humid regions; however, for semiarid to arid regions such as the Great Basin, Daymet's assumption of T_{dew} equaling T_{min} is largely inaccurate; therefore, Daymet T_{dew} estimates are compromised.

To examine the ability of daily GDPs to capture measured daily variability of temperature and precipitation, R^2

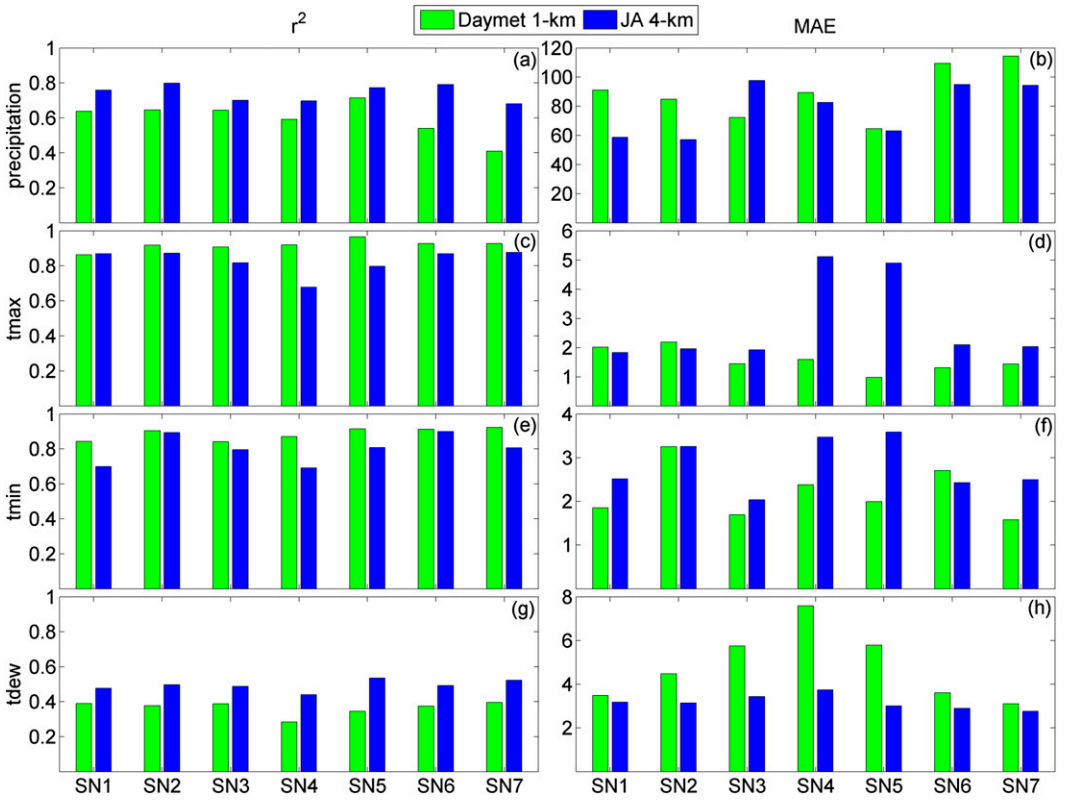

FIG. 9. Snake Range cold season (left) R^2 and (right) MAE computed at the daily time step for precipitation (a),(b) precipitation; (c),(d) T_{max}; (e),(f) T_{min}; and (g),(h) T_{dew} using Daymet and JA. For precipitation, MAE is expressed as a percentage, while MAE for T_{max}, T_{min}, and T_{dew} is expressed in degrees Celsius.

and MAE were computed for cold and warm seasons using Daymet and JA GDPs (Figs. 9, 10). Fairly good agreement was found between measured and estimated precipitation events during the cold season (Figs. 9a,b), with JA consistently having higher R^2 (0.68–0.80) and smaller MAE (58%–98%) when compared to Daymet (R^2 of 0.41–0.71, MAE of 65%–114%). Contrasting results were found with warm season precipitation (Figs. 10a,b), with generally much lower correlations, and higher MAE. Gridded data appear to be generating more daily misses (GDP = 0 and observed > 0) and false alarms (GDP > 0 and observed = 0) during the late spring and summer months (not shown). The nature of warm season precipitation events is typically convective and associated with a monsoonal pattern, which leads to a sporadic and nonuniform spatial distribution and lower correlations between GDPs and observations.

Daymet showed higher R^2 and lower MAE for T_{max} (Figs. 9c,d and 10c,d) and T_{min} (Figs. 9e,f and 10e,f) at most locations; however, differences between JA and Daymet error statistics were often times marginal. In general, higher MAE values were found with T_{min}, which is consistent with our seasonal results that highlight the weakness in GPDs to simulate inversion strength. The downscaling of the 32-km NARR temperature data to the 12-km NLDAS grid, and finally to the 4-km JA grid, is likely leading to larger error when compared to Daymet, where observations are interpolated directly to a 1-km grid. Not surprisingly, JA T_{dew} correlations were higher and MAE was lower than Daymet, especially during the warm season (Figs. 9g,h and 10g,h). This is largely a reflection of the assumptions used in the Daymet algorithm ($T_{min} = T_{dew}$). It should be noted that the calculation of T_{dew} from daily data with JA and Daymet is a contributing source of error when compared to NevCAN T_{dew} that was computed with 10-min data. Large differences were found at the daily time step when comparing NevCAN T_{dew} from 10-min data to T_{dew} from daily data, and differences often times exceeded 3°C day^{-1} (not shown).

c. *Sheep Range comparisons of observations and GDPs*

As discussed in section 2a, tipping buckets largely undermeasure precipitation during the cold season, and therefore, Sheep Range tipping-bucket measurements (Table 1, Figs. 11a,b) must be considered inaccurate at

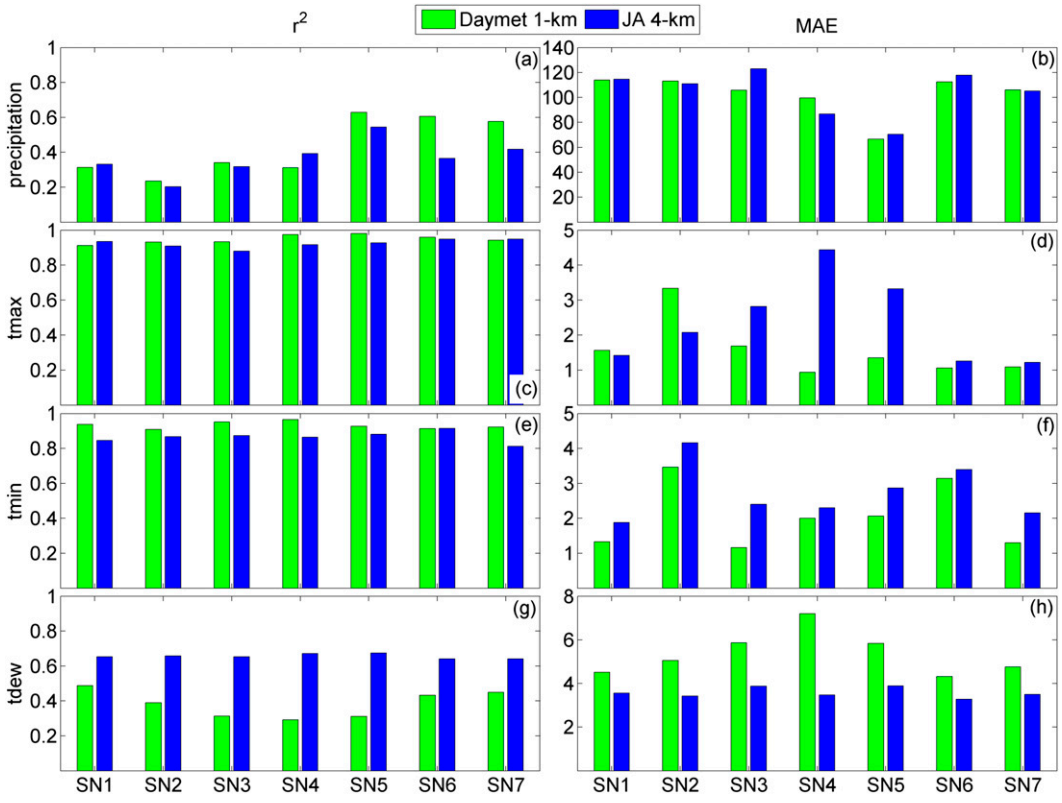

FIG. 10. As in Fig. 9, but for warm season.

the daily time step (and biased low). Unfortunately, all Sheep Range stations are equipped with tipping buckets only, except for SH4. Based on the assumption that frozen precipitation will occur at temperatures of less than 0°C, SH1 and YG were the only stations where all precipitation events were classified as liquid during both seasons. When considering the remaining four stations, a minimum of 38% of daily precipitation events were classified as frozen during the cold season at SH2 and a maximum of 91% at HP. Therefore, SH2, SH3, and HP cold season precipitation measurements contain the highest degree of uncertainty.

Differences between GDPs and observed precipitation were primarily positive (wet) during the cold season (Fig. 12a). Tipping-bucket deficiencies are likely causing undermeasurement at SH2, SH3, and HP, but this does not explain the large differences found with JA, PRISM 800 m, and Daymet at SH4 (41.69, 59.93, and 71.54 mm, respectively), where precipitation measurements came from the Geonor weighing gauge. This indicates that the instrumentation is likely not the only source of uncertainty. An additional source of error in the comparisons may be due to the fact that the nearest source of input data for GDPs in the region comes from the Spring Mountains (southwest of the Sheep Range), which are considerably wetter than the Sheep Range. During the warm season (when less uncertainty in tipping-bucket measurements exists), GDP seasonal precipitation totals were lower than observed at SH1, SH3, and SH4 and higher than observed at SH2, with mixed results at YG and HP (Fig. 12b). Large station-to-station variability was found with respect to differences between GDP and observed seasonal totals. For example, during the warm season at SH2, PRISM 800 m was found to have the greatest difference (75.1 mm) and Daymet had the smallest difference (26.57 mm), whereas the opposite was found at SH3, with PRISM 800 m having the smallest difference (−2.4 mm) and Daymet having the largest difference (−64.8 mm).

Maximum temperature biases during the cold season (Fig. 12c) ranged from −1.67° (JA) to 5.77°C (JA) and from −2.11° (JA) to 4.33°C (JA) during the warm season (Fig. 12d). The consistently large warm biases found at HP can be primarily explained by the large differences found between GDP and station elevations, with GDP elevations being −88 to −422 mm lower than the HP station elevation.

Observed seasonal mean T_{min} (Figs. 11e,f) was found to have similar characteristics as the Snake Range, with the alluvial fan station (YG) being warmer than the

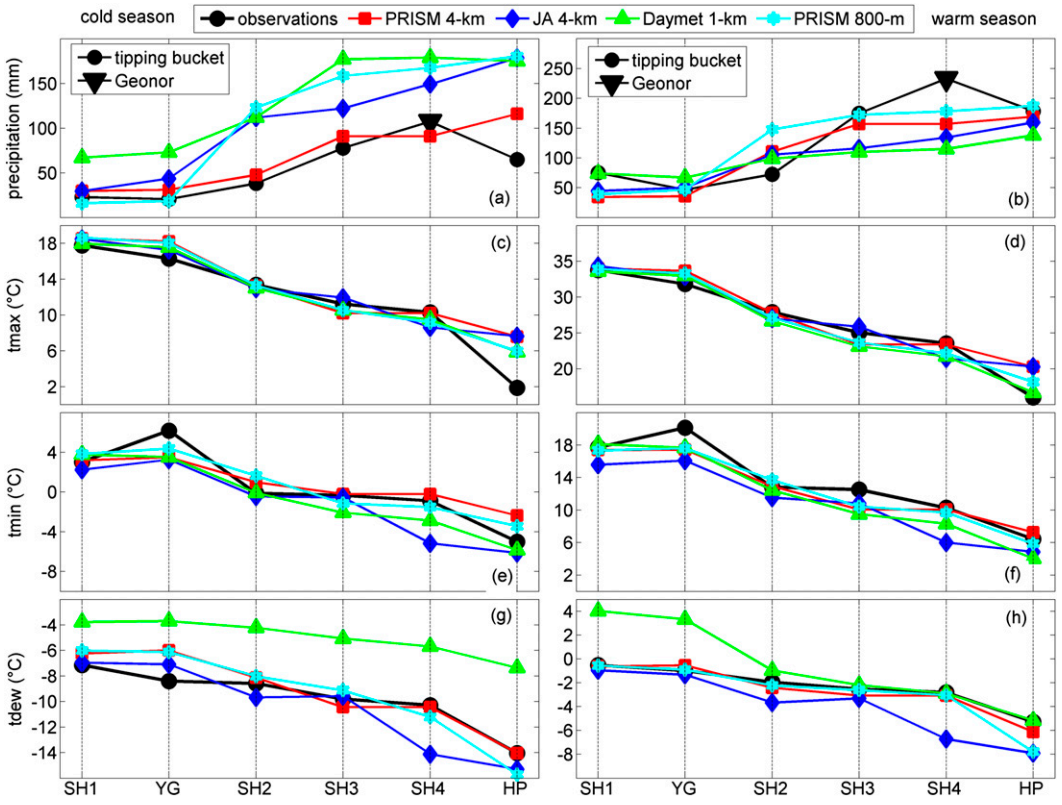

FIG. 11. Sheep Range seasonal (a),(b) PPT and mean (c),(d) T_{max}; (e),(f) T_{min}; and (g),(h) T_{dew} for (left) cold and (right) warm season. The x axis is aligned west–east (from left to right). For precipitation observations, filled circles represent tipping-bucket gauges and filled inverted triangles represent weighing gauges.

lower-elevation valley floor station (SH1) during both seasons. Daymet was the only GDP to not capture the cold air drainage feature. This highlights the importance of accounting for complex, nonmonotonic altitudinal gradients and temperature inversions, which are common throughout the Great Basin. Seasonal mean T_{min} biases during the cold season (Fig. 12e) ranged from −4.28° (JA) to 2.64°C (PRISM 4 km) and from −4.26° (JA) to 0.88°C (PRISM 800 m) during the warm season (Fig. 12f). As found at the Snake Range, T_{min} biases are not directly related to differences between GDP and station elevations. For example, cold biases were found at HP with JA and Daymet during both seasons, although the GDP elevations were lower than the station elevation (−335 and −88 m, respectively).

Both observed and GDP-estimated seasonal mean T_{dew} was found to decrease with altitude (Figs. 11g,h). This is in contrast to the Snake Range, where Daymet T_{dew} was found to increase with altitude during the warm season. Little consistency was found in GDP seasonal mean T_{dew} biases (Figs. 12g,h), with the exception of Daymet showing a consistent and large positive (warm) bias during the cold season, ranging from 3.42° to 6.63°C.

Daily precipitation error statistics for the Sheep Range (Figs. 13a,b and 14a,b) showed JA to have higher correlations and lower MAE at all stations during both seasons. At several locations during the cold season (SH1, YG, SH2, and HP), Daymet R^2 was low (<0.1) and MAE was high (>300%), while JA R^2 generally remained above 0.4. This may be partly because of the additional information regarding hourly precipitation that NLDAS-2 obtains from radar, satellite, and NARR, whereas Daymet relies only on station data and underlying regression relationships. The poor correlations in the cold season are partly due to tipping-bucket measurements, while additional uncertainty comes from a lack of GDP station data input in this region. It should also be noted that in this arid climate, precipitation occurs on only a small fraction of days (i.e., an average of 13% of days in the cold season), so correlations will decrease rapidly for each day that GDPs do not match observed precipitation. The combination of no GDP input from surface observations in the Sheep range, and primarily tipping-bucket rain gauges, leads to great uncertainty in both GDP estimates and NevCAN observations of precipitation in the Sheep Range.

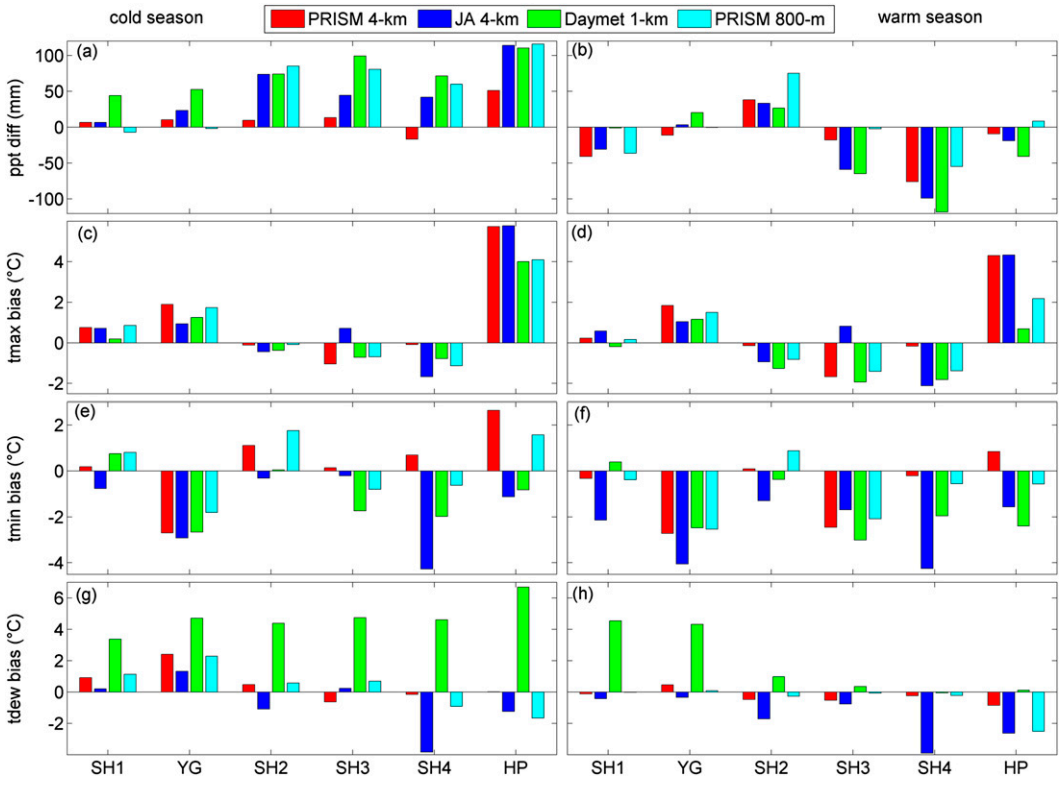

FIG. 12. Sheep Range seasonal bias (GDP minus obs) for (left) cold and (right) warm season (a),(b) PPT; (c),(d) T_{max}; (e),(f) T_{min}; and (g),(h) T_{dew}.

Daymet and JA T_{max} correlations (Figs. 13c, 14c) were quite similar and indicate good agreement to observations (R^2 is always >0.82), and the noticeably higher MAE at HP (Figs. 13d, 14d) could be attributed to the large differences between grid cell and station elevation. For T_{min}, error statistics were generally still good, but lower than T_{max}, which is again due to GDP errors with inversions. Daily T_{dew} error statistics (Figs. 13g,h and 14g,h) were consistent with the Snake Range, with JA always indicating less error than Daymet because of previously described deficiencies.

4. Summary and conclusions

In this study, we utilized the Nevada Climate-Ecohydrological Assessment Network (NevCAN) data to quantify altitudinal gradients of precipitation, maximum and minimum temperature (i.e., T_{max} and T_{min}), and dewpoint temperature (i.e., T_{dew}) along a west–east transect in the Snake Range and a south–north transect in the Sheep Range. NevCAN and additional observations were used to evaluate four gridded data products (GDPs) of varying spatial resolution (from 4 km to 800 m).

We have highlighted the challenges of providing reliable ''ground truth'' for evaluating GDP precipitation estimates in remote areas. By identifying large differences in water-year (2012) precipitation totals between SN5 and the Wheeler Peak SNOTEL (WPS) station (161 mm) and through the comparison of tipping-bucket and weighing gauge measurements presented in section 3a, we have highlighted several difficulties associated with comparing measurements of precipitation to GDP estimates of precipitation. The high GDP totals that were found with respect to NevCAN totals may largely be due to WPS being the only GDP input in the Snake Range. At the Sheep Range, perceived GDP ''overestimation'' is partly due to the use of tipping-bucket rain gauges as the source of baseline NevCAN measurements used for comparison. A second contribution to the large differences between GDPs and Sheep Range observed precipitation is due to the lack of any stations in the Sheep Range being used as GDP input. Potential users of gridded precipitation data should be aware that large uncertainty exists where station density is low, and especially when considering small, remote mountain ranges with no observations used as GDP input (such as the Sheep Range). It is highly recommended that any observing network with automated precipitation measurements be equipped with weighing-type gauges and wind shields, as this work and previous

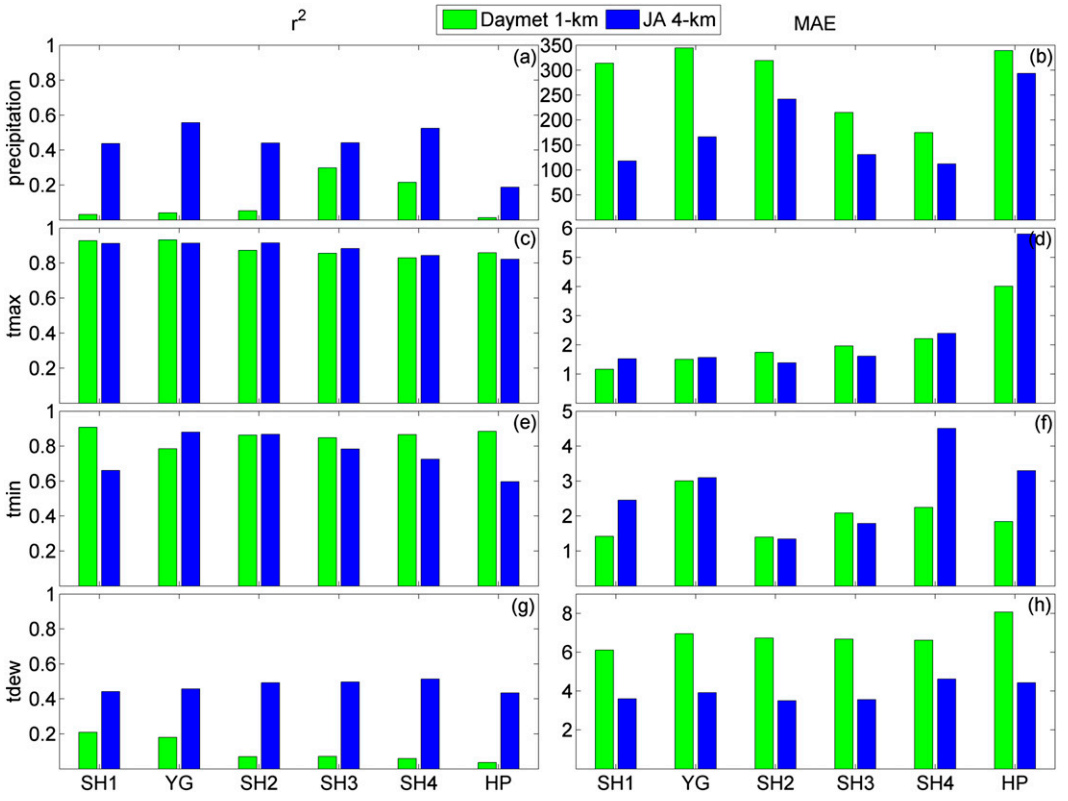

FIG. 13. Sheep Range cold season (left) R^2 and (right) MAE computed at the daily time step for (a),(b) precipitation; (c),(d) T_{max}; (e),(f) T_{min}; and (g),(h) T_{dew} using Daymet and JA. For precipitation, MAE is expressed as a percentage, while MAE for T_{max}, T_{min}, and T_{dew} is expressed in degrees Celsius.

studies (e.g., Humphrey et al. 1997; Rasmussen et al. 2012) have noted large errors associated with tipping-bucket measurements.

A key finding of this study was that temperature inversions at the alluvial fan locations were identified at both NevCAN transects, highlighting the importance of mountain transect observation networks. These findings are consistent with previous research that has identified cold air drainage as being the cause of this inverted T_{min}–elevation relationship (Gustavsson et al. 1998; Daly et al. 2010; Holden et al. 2011). The only GDP not able to replicate this temperature feature was Daymet; however, the magnitude of the T_{min} inversions observed at the Snake Range (mean monthly lapse rates of $>+15°C\,km^{-1}$ in some cases) was not estimated well by any GDP. Both Daymet and PRISM use local linear regressions of climate and elevation. However, the slope of the PRISM regression line can vary sharply with elevation, based on local inversion height and topographic position information. In contrast, the Daymet regression function is monotonic through the entire elevation range (Daly 2006). Given that maximum temperature showed a strong relationship with elevation, biases between GDPs and observations were strongly related to differences between GDP and station elevation. In general, PRISM 800 m and Daymet contained smaller biases than PRISM 4 km and JA for both T_{max} and T_{min}, indicating that spatial resolution of less than 4 km can provide valuable details regarding temperature features.

We have highlighted a limitation of using an overly simplistic estimation for T_{dew} (T_{min} equals daily average T_{dew}) in semiarid to arid environments, which results in an unrealistic increase of T_{dew} with elevation in the Snake Range and generally a large bias compared to observations of T_{dew}. The combination of Daymet's assumption of T_{min} equals daily average T_{dew} and the inability to reproduce temperature inversions make the application of Daymet to estimate humidity levels in semiarid and arid areas largely uncertain. Reasonable T_{dew} estimates were provided by PRISM and JA. However, the calculation of T_{dew} from JA and Daymet daily data was a contributing source of error when comparing these estimates to NevCAN T_{dew}, which was computed with 10-min data.

This research highlights the importance of conducting local analyses of observations and potential measurement errors to gain an understanding of potential GDP biases prior to use in hydroclimatic applications. Although local

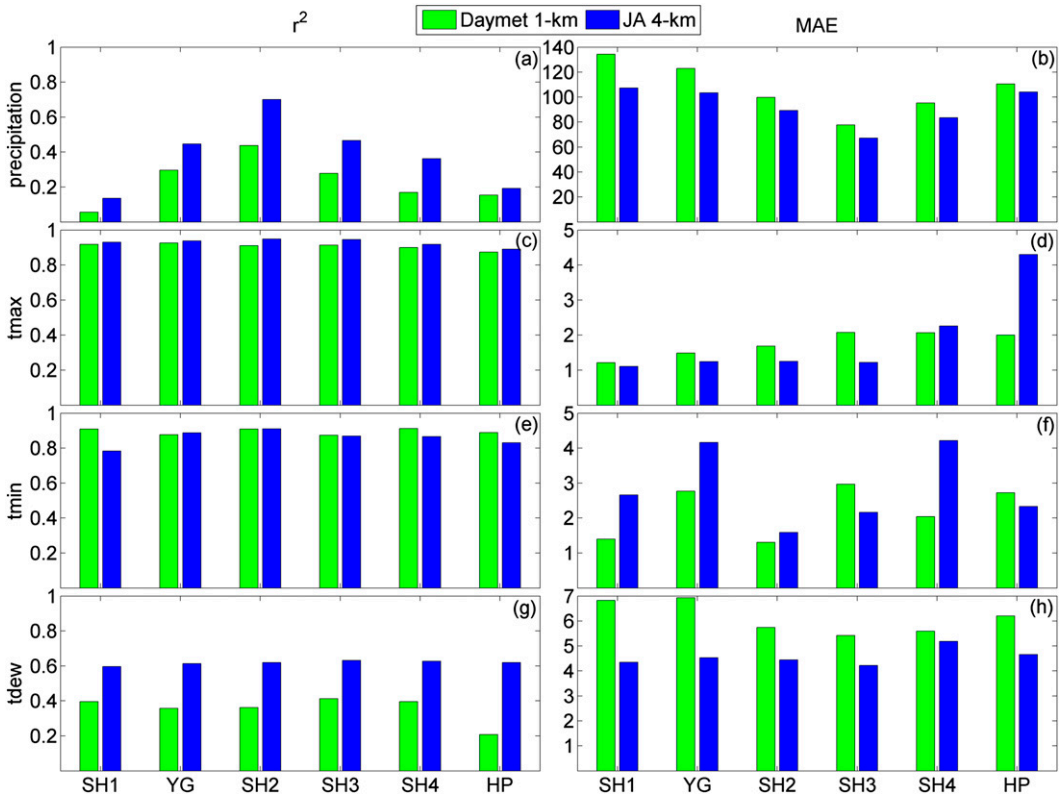

FIG. 14. As in Fig. 13, but for warm season.

results may vary, this work compliments other hydroclimatic studies throughout the Great Basin region where geographical attributes are similar to the NevCAN transects. Procedures and results from this study are useful for improving our understanding of GDP evaluation and analyses related to hydroclimatic assessments in semiarid and arid climates.

Acknowledgments. The authors thank three anonymous reviewers for helping to improve this manuscript through constructive feedback. We would also like to acknowledge Greg McCurdy, Dr. Lynn Fenstermaker, Brad Lyles, and Dr. Jay Arnone for their valuable contributions regarding the NevCAN instrumentation and site characteristics. This work was partially funded by National Science Foundation under Grant EPS-0814372 and by the Desert Research Institute Divisions of Atmospheric Science and Hydrologic Science faculty and graduate research. The work was also funded by Landsat Science Team funding under USGS Grant G12PC00068 and the U.S. Bureau of Reclamation Nevada Water Resources Evaluation Program in collaboration with the Nevada State Engineer's Office, funded by a grant under Public Law 109-103, Section 208 (a), Cooperative Agreement 06FC204044.

REFERENCES

Abatzoglou, J. T., 2013: Development of gridded surface meteorological data for ecological applications and modeling. *Int. J. Climatol.,* **33,** 121–131, doi:10.1002/joc.3413.

Ackerly, D. D., S. R. Loarie, W. K. Cornwell, S. B. Weiss, H. Hamilton, R. Branciforte, and N. J. B. Kraft, 2010: The geography of climate change: Implications for conservation biogeography. *Diversity Distrib.,* **16,** 476–487, doi:10.1111/j.1472-4642.2010.00654.x.

Allen, R. G., L. S. Pereira, D. Raes, and M. Smith, 1998: Crop evapotranspiration: Guidelines for computing crop water requirements. FAO Irrigation and Drainage Paper 56, 300 pp. [Available online at www.fao.org/docrep/X0490E/X0490E00.htm.]

Alter, J. C., 1937: Shielded storage precipitation gages. *Mon. Wea. Rev.,* **65,** 262–265, doi:10.1175/1520-0493(1937)65<262:SSPG>2.0.CO;2.

Bandyopadhyay, J., and Coauthors, 1997: Highland waters: A resource of global significance. *Mountains of the World: A Global Priority,* B. Messerli and J. D. Ives, Eds., Parthenon, 131–155.

Barnett, T. P., J. C. Adam, and D. P. Lettenmaier, 2005: Potential impacts of a warming climate on water availability in snow-dominated regions. *Nature,* **438,** 303–309, doi:10.1038/nature04141.

Bradley, B. A., 2009: Regional analysis of the impacts of climate change on cheatgrass invasion shows potential risk and opportunity. *Global Change Biol.,* **15,** 196–208, doi:10.1111/j.1365-2486.2008.01709.x.

Burns, A. G., and W. Drici, 2011: Hydrology and water resources of Spring, Cave, Dry Lake, and Delamar Valleys, Nevada and vicinity. Southern Nevada Water Authority, Las Vegas, NV, 313 pp.

Cosgrove, B. A., and Coauthors, 2003: Real-time and retrospective forcing in the North American Land Data Assimilation System (NLDAS) project. *J. Geophys. Res.,* **108,** 8842, doi:10.1029/2002JD003118.

Crago, R. D., R. J. Qualls, and M. Feller, 2010: A calibrated advection–aridity evaporation model requiring no humidity data. *Water Resour. Res.,* **46,** W09519, doi:10.1029/2009WR008497.

Daly, C., 2006: Guidelines for assessing the suitability of spatial climate data sets. *Int. J. Climatol.,* **26,** 707–721, doi:10.1002/joc.1322.

——, R. P. Neilson, and D. L. Phillips, 1994: A statistical–topographic model for mapping climatological precipitation over mountainous terrain. *J. Appl. Meteor.,* **33,** 140–158, doi:10.1175/1520-0450(1994)033<0140:ASTMFM>2.0.CO;2.

——, M. Halbleib, J. I. Smith, W. P. Gibson, M. K. Doggett, G. H. Taylor, J. Curtis, and P. P. Pasteris, 2008: Physiographically sensitive mapping of climatological temperature and precipitation across the conterminous United States. *Int. J. Climatol.,* **28,** 2031–2064, doi:10.1002/joc.1688.

——, D. R. Conklin, and M. H. Unsworth, 2010: Local atmospheric decoupling in complex topography alters climate change impacts. *Int. J. Climatol.,* **30,** 1857–1864, doi:10.1002/joc.2007.

Eakin, T. E., 1966: A regional interbasin ground-water system in the White River area, southeastern Nevada. *Water Resour. Res.,* **2,** 251–271, doi:10.1029/WR002i002p00251.

Epstein, B. J., G. M. Pohll, J. Huntington, and R. W. H. Carroll, 2010: Development and uncertainty analysis of an empirical recharge prediction model for Nevada's desert basins. *Journal of the Nevada Water Resources Association,* Vol. 5, Issue 1, Nevada Water Resources Association, 1–22. [Available online at www.dri.edu/images/stories/divisions/dhs/dhsfaculty/Justin-Huntington/Epstein_et_al_2010.pdf.]

Fassnacht, S. R., 2004: Estimating Alter-shielded gauge snowfall undercatch, snowpack sublimation, and blowing snow transport at six sites in the coterminous USA. *Hydrol. Processes,* **18,** 3481–3492, doi:10.1002/hyp.5806.

Feld, S. I., N. C. Cristea, and J. D. Lundquist, 2013: Representing atmospheric moisture content along mountain slopes: Examination using distributed sensors in the Sierra Nevada, California. *Water Resour. Res.,* **49,** 4424–4441, doi:10.1002/wrcr.20318.

Flint, A. L., L. E. Flint, J. A. Hevesi, and J. M. Blainey, 2004: Fundamental concepts of recharge in the desert Southwest: A regional modeling perspective. *Groundwater Recharge in a Desert Environment: The Southwestern United States,* J. F. Hogan, F. M. Phillips, and B. R. Scanlon, Water Science and Application Series, Vol. 9, Amer. Geophys. Union, 159–184.

Goodison, B. E., P. Y. T. Louie, and D. Yang, 1998: WMO solid precipitation measurement intercomparison. WMO Instruments and Observing Methods Rep. 67, WMO/TD 872, 2011 pp. [Available online at www.wmo.int/pages/prog/www/IMOP/publications/IOM-67-solid-precip/WMOtd872.pdf.]

Gustavsson, T., M. Karlsson, J. Bogren, and S. Lindqvist, 1998: Development of temperature patterns during clear nights. *J. Appl. Meteor.,* **37,** 559–571, doi:10.1175/1520-0450(1998)037<0559:DOTPDC>2.0.CO;2.

Holden, Z. A., J. T. Abatzoglou, L. S. Baggett, and C. Luce, 2011: Empirical downscaling of daily minimum air temperature at very fine resolutions in complex terrain. *Agric. For. Meteor.,* **151,** 1066–1073, doi:10.1016/j.agrformet.2011.03.011.

Houghton, J. G., 1979: A model for orographic precipitation in the north-central Great Basin. *Mon. Wea. Rev.,* **107,** 1462–1475, doi:10.1175/1520-0493(1979)107<1462:AMFOPI>2.0.CO;2.

Humphrey, M. D., J. D. Istok, J. Y. Lee, A. Hevesi, and A. L. Flint, 1997: A new method for automated dynamic calibration of tipping-bucket rain gauges. *J. Atmos. Oceanic Technol.,* **14,** 1513–1519, doi:10.1175/1520-0426(1997)014<1513:ANMFAD>2.0.CO;2.

Huntington, J. L., and D. J. McEvoy, 2011: Climatological estimates of open water evaporation from selected Truckee and Carson River basin water bodies, California and Nevada. Desert Research Institute Publ. 41254, 35 pp. [Available online at www.dri.edu/images/stories/divisions/dhs/dhsfaculty/Justin-Huntington/Huntington_and_McEvoy_2011.pdf.]

——, and R. G. Niswonger, 2012: Role of surface-water and groundwater interactions on projected summertime streamflow in snow dominated regions: An integrated modeling approach. *Water Resour. Res.,* **48,** W11524, doi:10.1029/2012WR012319.

——, J. L. Szilagyi, S. W. Tyler, and G. M. Pohll, 2011: Evaluating the complementary relationship for estimating evapotranspiration from arid shrublands. *Water Resour. Res.,* **47,** W05533, doi:10.1029/2010WR009874.

Jeton, A. E., S. A. Watkins, T. J. Lopes, and J. L. Huntington, 2006: Evaluation of precipitation estimates from PRISM for the 1961–90 and 1971–2000 data sets, Nevada. USGS Scientific Investigations Rep. 2005-5291, 25 pp. [Available online at http://pubs.usgs.gov/sir/2005/5291/PDF/SIR2005_5291.pdf.]

Leger, E. A., 2013: Annual plants change in size over a century of observations. *Global Change Biol.,* **19,** 2229–2239, doi:10.1111/gcb.12208.

Loarie, S. R., P. B. Duffy, H. Hamilton, G. P. Asner, C. B. Field, and D. D. Ackerly, 2009: The velocity of climate change. *Nature,* **462,** 1052–1055, doi:10.1038/nature08649.

Lundmark, K. W., G. M. Pohll, and R. W. H. Carroll, 2007: A steady-state water budget accounting model for the carbonate aquifer system in White Pine County, Nevada, and adjacent areas in Nevada and Utah. Desert Research Institute Publ. 41235, 56 pp. [Available online at www.dri.edu/images/stories/research/projects/BARCAS/41235_2007_barcas_dsc_report.pdf.]

Lundquist, J. D., J. R. Minder, P. J. Neiman, and E. Sukovich, 2010: Relationship between barrier jet heights, orographic precipitation gradients, and streamflow in the northern Sierra Nevada. *J. Hydrometeor.,* **11,** 1141–1156, doi:10.1175/2010JHM1264.1.

McEvoy, D. J., J. L. Huntington, J. T. Abatzoglou, and L. M. Edwards, 2012: An evaluation of multiscalar drought indices in Nevada and eastern California. *Earth Interact.,* **16,** doi:10.1175/2012EI000447.1.

Mensing, S., and Coauthors, 2013: A network for observing Great Basin climate change. *Eos, Trans. Amer. Geophys. Union,* **94,** 105–106, doi:10.1002/2013EO110001.

Mesinger, F., and Coauthors, 2006: North American Regional Reanalysis. *Bull. Amer. Meteor. Soc.,* **87,** 343–360, doi:10.1175/BAMS-87-3-343.

Mitchell, K. E., and Coauthors, 2004: The multi-institution North American Land Data Assimilation System (NLDAS): Utilizing multiple GCIP products and partners in a continental distributed hydrological modeling system. *J. Geophys. Res.,* **109,** D07S90, doi:10.1029/2003JD003823.

Murray, F. W., 1967: On the computation of saturation vapor pressure. *J. Appl. Meteor.,* **6,** 203–204, doi:10.1175/1520-0450(1967)006<0203:OTCOSV>2.0.CO;2.

Nevada Bureau of Land Management, 2012: Purpose and need for this federal action. Clark, Lincoln, and White Pine Counties Groundwater Development Project Final Environmental Impact Statement, 1–21. [Available online at www.blm.gov/nv/st/en/prog/planning/groundwater_projects/snwa_groundwater_project/final_eis.html.]

Nevada State Engineer's Office, 2012: Ruling 6164, in the matter of applications 54003 through 54021, inclusive, filed to appropriate the underground waters of the Spring Valley hydrographic basin (184), Lincoln and White Pine Counties, Nevada, 218 pp. [Available online at www.snwa.com/assets/pdf/ws_gdp_spring_ruling_2012.pdf.]

Porinchu, D. F., S. Reinemann, B. G. Mark, J. E. Box, and N. Rolland, 2010: Application of a midge-based inference model for air temperature reveals evidence of late-20th century warming in sub-alpine lakes in the central Great Basin, United States. *Quat. Int.,* **215,** 15–26, doi:10.1016/j.quaint.2009.07.021.

Rangwala, I., and J. R. Miller, 2012: Climate change in mountains: A review of elevation-dependent warming and its possible causes. *Climatic Change,* **114,** 527–547, doi:10.1007/s10584-012-0419-3.

Rasmussen, R., and Coauthors, 2012: How well are we measuring snow? The NOAA/FAA/NCAR winter precipitation test bed. *Bull. Amer. Meteor. Soc.,* **93,** 811–829, doi:10.1175/BAMS-D-11-00052.1.

Rauscher, S. A., J. S. Pal, N. S. Diffenbaugh, and M. M. Benedetti, 2008: Future changes in snowmelt-driven runoff timing over the western US. *Geophys. Res. Lett.,* **35,** L16703, doi:10.1029/2008GL034424.

Sieck, L. C., S. J. Burges, and M. Steiner, 2007: Challenges in obtaining reliable measurements of point rainfall. *Water Resour. Res.,* **43,** W01420, doi:10.1029/2005WR004519; Corrigendum, **43,** W06701, doi:10.1029/2007WR005985.

Smith, R. B., 1979: The influence of mountains on the atmosphere. *Advances in Geophysics,* Vol. 21, Academic Press, 87–230, doi:10.1016/S0065-2687(08)60262-9.

Thornton, P. E., and S. W. Running, 1999: An improved algorithm for estimating incident daily solar radiation from measurements of temperature, humidity, and precipitation. *Agric. For. Meteor.,* **93,** 211–228, doi:10.1016/S0168-1923(98)00126-9.

——, ——, and M. A. White, 1997: Generating surfaces of daily meteorology variables over large regions of complex terrain. *J. Hydrol.,* **190,** 214–251, doi:10.1016/S0022-1694(96)03128-9.

——, H. Hasenauer, and M. A. White, 2000: Simultaneous estimation of daily solar radiation and humidity from observed temperature and precipitation: An application over complex terrain in Austria. *Agric. For. Meteor.,* **104,** 255–271, doi:10.1016/S0168-1923(00)00170-2.

——, M. M. Thornton, B. W. Mayer, N. Wilhelmi, Y. Wei, R. Devarakonda, and R. B. Cook, 2014: Daymet: Daily surface weather on a 1-km grid for North America, version 2. ORNL Distributed Active Archive Center, Oak Ridge, TN, doi:10.3334/ORNLDAAC/Daymet_V2.

Welch, A. H., D. J. Bright, and L. A. Knochenmus, Eds., 2007: Water resources of the Basin and Range carbonate-rock aquifer system, White Pine County, Nevada, and adjacent areas in Nevada and Utah. USGS Scientific Investigations Rep. 2007–5261, 96 pp. [Available online at http://pubs.usgs.gov/sir/2007/5261/.]

Willmott, C. J., and S. M. Robeson, 1995: Climatologically aided interpolation (CAI) of terrestrial air temperature. *Int. J. Climatol.,* **15,** 221–229, doi:10.1002/joc.3370150207.

Yang, D., B. E. Goodison, and J. R. Metcalfe, 1998: Accuracy of NWS 8'' standard nonrecording precipitation gauge: Results and application of WMO intercomparison. *J. Atmos. Oceanic Technol.,* **15,** 54–68, doi:10.1175/1520-0426(1998)015<0054:AONSNP>2.0.CO;2.

Zhu, J., and M. H. Young, 2009: Sensitivity and uncertainty of ground-water discharge estimates for semiarid shrublands. *J. Amer. Water Resour. Assoc.,* **45,** 641–653, doi:10.1111/j.1752-1688.2009.00312.x.